

Trapezoidal Wing Experimental Repeatability and Velocity Profiles in the 14- by 22-Foot Subsonic Tunnel (Invited)

Judith A. Hannon,^{*} Anthony E. Washburn,[†] Luther N. Jenkins,[‡] Ralph D. Watson[§]
NASA Langley Research Center, Hampton, VA 23681

The AIAA Applied Aerodynamics Technical Committee sponsored a High Lift Prediction Workshop held in June 2010. For this first workshop, data from the Trapezoidal Wing experiments were used for comparison to CFD. This paper presents long-term and short-term force and moment repeatability analyses for the Trapezoidal Wing model tested in the NASA Langley 14- by 22-Foot Subsonic Tunnel. This configuration was chosen for its simplified high-lift geometry, publicly available set of test data, and previous CFD experience with this configuration. The Trapezoidal Wing is a three-element semi-span swept wing attached to a body pod. These analyses focus on configuration 1 tested in 1998 (Test 478), 2002 (Test 506), and 2003 (Test 513). This paper also presents model velocity profiles obtained on the main element and on the flap during the 1998 test. These velocity profiles are primarily at an angle of attack of 28 degrees and semi-span station of 83% and show confluent boundary layers and wakes.

Nomenclature

12 Foot	=	NASA Ames Research Center 12-Foot Pressure Wind Tunnel
14x22	=	NASA Langley Research Center 14- by 22-Foot Subsonic Tunnel
B.L.	=	boundary layer
BLRS	=	boundary layer removal system
c	=	local stowed chord, inches
C_D	=	drag coefficient
C_L	=	lift coefficient
C_m	=	pitching moment coefficient, reference point is the 1/4 chord of the stowed mean aerodynamic chord
g/c	=	slat gap or flap gap, non-dimensionalized by local stowed chord
h/c	=	slat height, non-dimensionalized by local stowed chord
h_{probe}	=	7-hole probe heights normal to the local surface, inches
HiLiftPW	=	High Lift Prediction Workshop
M	=	free-stream Mach number
MAC	=	stowed mean aerodynamic chord, inches
o/c	=	flap overlap, non-dimensionalized by local stowed chord
pred int	=	prediction interval
q_∞	=	free-stream dynamic pressure, pounds per square foot
Re_c	=	free-stream Reynolds number based on stowed mean aerodynamic chord
S_{ref}	=	wing reference area based on stowed semi-span wing to bottom of body pod, square feet
T478	=	14x22 Test 478 (conducted in 1998)
T506	=	14x22 Test 506 (conducted in 2002)
T513	=	14x22 Test 513 (conducted in 2003)
v	=	spanwise velocity component, feet per second
V_∞	=	tunnel free-stream velocity, feet per second

^{*} Aerospace Engineer, Flow Physics & Control Branch, Mail Stop 170

[†] Aerospace Engineer, Flow Physics & Control Branch, Mail Stop 170, Senior Member AIAA

[‡] Aerospace Engineer, Flow Physics & Control Branch, Mail Stop 170

[§] Retired, Senior Member AIAA

- x = model coordinate, inches
 y = model coordinate, inches
 z = model coordinate, inches

 α = angle of attack, degrees
 η = spanwise location, non-dimensionalized by the semi-span length (85.054 inches), relative to bottom of body pod, i.e., does not include 0.95 inch standoff that is included in the CFD geometry
 Δ = difference between curve fit and data point value

I. Introduction

The AIAA Applied Aerodynamics Technical Committee sponsored a High Lift Prediction Workshop^{1,2} (HiLiftPW-1) held in June 2010. The objectives of the workshop were to

- Assess the numerical prediction capability (meshing, numerics, turbulence modeling, high-performance computing requirements, etc.) of current-generation CFD technology/codes for swept, medium-to-high-aspect ratio wings for landing/take-off (high-lift) configurations.
- Develop practical modeling guidelines for CFD prediction of high-lift flow fields.
- Advance the understanding of high-lift flow physics to enable development of more accurate prediction methods and tools.
- Enhance CFD prediction capability for practical high-lift aerodynamic design and optimization.

Details of the first workshop and continuing work for High Lift Prediction Workshops can be accessed from the HiLiftPW website.[‡]

For this first workshop, data from the Trapezoidal Wing (Trap Wing) experiments were used for comparison to CFD. This configuration was chosen for its non-proprietary, simplified high-lift geometry; publicly available set of test data; and previous CFD studies using this configuration. The Trapezoidal Wing is a three-element semi-span swept wing attached to a body pod. Even though this is a "simplified" three-dimensional geometry, the Trap Wing flow field contains relevant flow phenomena associated with a high-lift system. These include "laminar flow, attachment line transition, transonic slat flow, confluent boundary layers, wake interactions, separation, and reattachment."³ Figure 1 shows some relevant high-lift flow features.

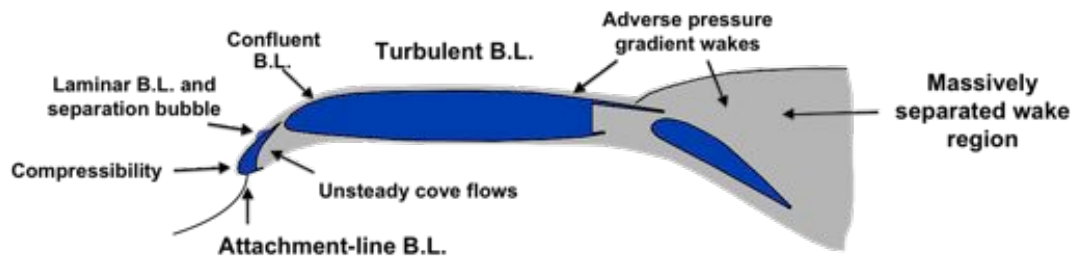


Figure 1. High-lift flow physics.

This paper presents long-term and short-term force and moment repeatability analyses for the Trapezoidal Wing model tested in the NASA Langley 14- by 22-Foot Subsonic Tunnel (14x22). These analyses focus on the baseline, full-span flap, landing configuration (config 1) tested in 1998 (Test 478), 2002 (Test 506), and 2003 (Test 513). There are notable differences between the test entries and these will be discussed. The long-term repeatability analysis was done to provide experimental ranges of C_L , C_D , and C_m to the CFD community. These ranges were used during HiLiftPW-1 and included in the workshop summary paper.² They are also available on the HiLiftPW website.

‡ <http://hiliftpw.larc.nasa.gov>, accessed 9/9/2011

This paper also presents velocity profiles obtained during the 1998 test in the 14x22. Because of the renewed interest in the Trap Wing dataset due to the HiLiftPW activities there was the opportunity to evaluate previously unpublished velocity profiles from 1998. There are a limited number of profiles from the 14x22 entry. Many more profiles were taken during a 12 Foot entry in 1999 and these will be evaluated in the future. The velocity profiles presented are primarily at $\alpha = 28^\circ$ and $\eta = 83\%$ and located on the main element and on the flap.

II. Description of Experiments

This paper includes data from two experimental investigations that used the Trapezoidal Wing model. Wind tunnel testing for the first investigation occurred in 1998 (14x22) and 1999 (12 Foot) and this is generally referred to as the Trapezoidal Wing Experiment. The second investigation included wind tunnel testing in 2002 and 2003 (both in 14x22) and is referred to as the 3-D High-Lift Flow Physics Experiment. Both investigations were designed to assess CFD and experiment correlation on a three-dimensional, high-lift configuration. The first was designed to cover a range of configurations and a range of Reynolds numbers. The second was designed to focus on detailed flow physics data at one Reynolds number for one configuration.

A. Model Description

The Trap Wing is a simplified, three-dimensional, swept, low aspect ratio, non-proprietary, high-lift, semi-span model. The model consists of a full-span slat, a main element, either a full-span flap or a part-span flap, and a body pod. Even though the geometry is "simple" and the aspect ratio is lower than a typical transport, the model provides the relevant flow physics features for a high-lift flow field, such as massive separations, unsteady effects, strong streamline curvature, and transition. The Trap Wing model has also been used for airframe noise investigations in the 14x22.^{4,5}

The slat consists of three segments, each held to the main element with two brackets. All slat segments are deployed to the same settings. The full-span flap consists of a single segment and attaches to the main element with four brackets. The part-span flap consists of a single segment, which deploys from 26% semi-span to 75% semi-span and is held to the main element with two brackets. There are inboard and outboard cruise pieces to complete the part-span flap configuration.

The model has 700-800 surface static pressure orifices. All pressure tubing from the slat and flap run through the brackets and through the main element to pressure sensors either in the body pod or below the tunnel floor. At the base of the body pod is a standoff with a labyrinth seal to prevent airflow under the body pod. Table 1 contains model geometry parameters.

The model can be tested with a variety of deployed slat and deployed flap positions. This paper will focus on the baseline full-span flap landing configuration (designated as "config 1"). Config 1 deployed slat and flap parameters are listed in Table 2. Gaps, overlaps, and heights are non-dimensionalized by the local stowed chord length. Note that there is a difference in flap overlap between the two series of tests that will be discussed in the section on the 2002/2003 experimental investigation.

Table 1. Trap Wing geometry.

semi-span	85.054 inches
MAC	39.6 inches
aspect ratio	4.56
S_{ref}	22.028 square feet
leading edge sweep	33.9 deg
quarter chord sweep	30.0 deg
taper ratio	0.4
slat brackets, η	0.13, 0.33, 0.47, 0.64, 0.77, 0.94
flap brackets, η	0.13, 0.37, 0.61, 0.80

Table 2. Deployed settings for config 1.

slat deflection	30 degrees
slat gap (g/c)	0.015
slat height (h/c)	0.015
flap deflection	25 degrees
flap gap (g/c)	0.015
flap overlap (o/c)	0.005 (1998, 1999) or 0.0026 (2002, 2003)

B. 14- by 22-Foot Subsonic Tunnel Description

The 14x22 is a low speed, atmospheric, closed circuit tunnel with a test section of 14.5 feet high and 21.75 feet wide.⁶ The Mach number range is from 0 to 0.3. The facility can operate in a closed test section configuration or with walls and/or ceiling raised for 2 or 3 sided partially open configurations. The 14x22 has a boundary layer removal system (BLRS) on the floor at the beginning of the test section. The data presented in this paper were taken in the closed test section configuration and the BLRS was used to reduce the size of the tunnel floor boundary layer.

The 14x22 was designed for a variety of testing and the floor of the test section consists of removable model carts that provide various mechanisms for model movement in the test section. Over the years, new model carts have been added and others have evolved. This is relevant to the Trap Wing experiments because the cart used for model installation into the test section was changed between the 1998 test and the 2002 test. For the 1998 test, Cart 1 was modified to provide a temporary support for this semi-span model. Prior to the 2002 entry, Cart 2 was modified to have a permanent semi-span mount capability and this cart was used for the 2002 and 2003 tests. Cart 2 allowed a better centering of the model's rotation point on the turntable and this affected the streamwise location of the model in the test section. For all the Trap Wing tests in 14x22, rotating the turntable on the floor sets the model angle of attack.

C. 1998/1999 Experimental Investigation

This experimental investigation was designed to provide a set of data that would be useful for CFD validation over a variety of flow conditions from fully attached to significantly separated. The model was first tested in the



NASA Trapezoidal wing model
NASA Langley Research Center
9/15/1998 Image # EL-1998-00248

Figure 2. Trap Wing model installed in 14x22 during 1998 test.

Langley 14x22 in 1998 and then in the Ames 12 Foot tunnel in 1999. The NASA Advanced Subsonic Transport program supported this investigation and these were cooperative tests involving NASA, Boeing, and McDonnell-Douglas. This set of data was to include overall forces/moments, surface pressures, transition information, and mean velocity profiles.

The goal was to acquire data over a range of full-span flap and part-span flap configurations and over a range of Reynolds numbers. This investigation consisted of tests in two large wind tunnels. The first test was conducted in the 14x22 at a Reynolds number of approximately 4.3×10^6 (Fig. 2 shows the model in 14x22). The primary goal of this test was to get useable data from a tunnel with small wall effects and to downselect configurations for the 12 Foot entry. Another goal of this 14x22 entry was to provide risk reduction for the measurement techniques prior to the 12 Foot entry. The 12 Foot is a pressurized tunnel and was used to test the model over a range of Reynolds numbers, up to 15×10^6 . The 12 Foot data showed extensive blockage effects with this model and for CFD purposes it is necessary to model the wind tunnel.⁷ See Ref. 3 for a more detailed overview of this experimental investigation. There is a website with this data available that can currently be accessed through the HiLiftPW website.

D. 2002/2003 Experimental Investigation

Although the 3-D High-Lift Flow Physics Experiment used the Trap Wing model, it was a separate investigation from the tests conducted in 1998 and 1999. The Trap Wing model was chosen for this investigation for all of the same reasons mentioned for the 1998/1999 investigation. In addition there was experience dealing with this

particular model and its size was conducive to making detailed flow measurements. Because this was a separate investigation there are several differences in the setup from the 1998 entry that will be detailed in this section. This investigation was supported by the NASA Aerospace Systems Concept to Test (ASCOT) Project and then the Efficient Aerodynamics Shapes and Integration (EASI) Project.

There were three 14x22 entries dedicated to this investigation:

- Test 509 was conducted in July 2002 and focused on acquiring empty tunnel conditions without the model installed. Free-stream turbulence levels,⁸ tunnel wall boundary layer profiles, total and static pressure distributions, and flow angularity were measured.
- Test 506 was conducted in August 2002 and focused on obtaining boundary layer state and transition information on the slat, main element, and flap using hot films.⁹ Overall forces and moments, static surface pressures, model deformation and wing twist were also measured during this test. Figure 3 shows the model installed in 14x22 with hot films on the lower surface.
- Test 513 was conducted in March 2003 and focused on off-body flow field measurements using stereo particle imaging velocimetry (SPIV). All of the hot films were removed from the surface prior to this entry. This test also included measuring the overall forces and moments and static surface pressures again. The PIV data has not been completely processed; however, a description of the system and test setup can be found in Ref. 10.



Figure 3. Trap Wing model installed in 14x22 during 2002 test.

The model configuration chosen for this set of tests was the baseline full-span flap landing configuration, i.e., config 1. The configuration tested was slightly different than the 1998 configuration. The slat settings were the same and the flap deflection and gaps were the same. However, due to work on the model to install hot film cables, at a flap setting of 25° and g/c of 0.015, the overlap did not match the overlap from 1998. The researchers decided to keep the gap the same as 1998 and accept the difference in overlap. The o/c averaged 0.0026 over the span of the model for T506/T513 instead of 0.005 as it was for T478.

Several changes were made to the facility and to the model setup between the 1998 test and the 2002/2003 tests. The facility had a new tunnel drive installed, an extensive set of wall pressures added to the side walls and ceiling for use with the Transonic Wall Interference Correction System (TWICS),¹¹ a semi-span mount added to Cart 2, and a new suction surface⁸ for the boundary layer removal system installed.

The addition of the semi-span mount permitted the x location of the $1/4$ chord of the MAC to be closer to the center of the turntable which rotated to set angle of attack. For T506 and T513 this rotation point was the center of the balance which is approximately 5 inches in front of the $1/4$ chord of the MAC. In the 1998 test, the model was over 2 feet further upstream in the test section. This means

during the 1998 test, the model moved closer to the upper surface wall with increasing angle of attack, whereas during T506 and T513 the model was more centered in the tunnel with increasing angle of attack.

The strain gauge balance that measured the forces/moments was also changed for T506/T513. The physical dimensions of the balances were the same, but the load capability was increased for T506/T513.

E. Corrections Applied to the Data

The data in this paper were corrected for wind tunnel wall interference to "free-air" conditions. The corrections are classical wall corrections and two corrections are applied. The correction factors were calculated by treating the semi-span model as a full-span model in a tunnel of double the width. One is a correction to the free-stream tunnel conditions and the second is a correction to the model angle of attack. The first is a blockage correction¹² that accounts for the solid blockage of the model and for the wake blockage from the model. The wake blockage correction assumes an attached wake. The blockage correction corrects the tunnel velocity and other tunnel conditions, including the free-stream dynamic pressure, q_∞ . The q_∞ correction is less than 0.5% for most of the α range and increases to a maximum of 2.2% post-stall. The second correction due to the presence of the walls is a change to the average induced upwash¹³ at the model and corrects the model angle of attack, α . The correction to α increases from approximately 0.10 degrees to a maximum of approximately 1.45 degrees at the maximum lift coefficient, $C_{L,max}$.

These corrections are then implemented in the data reduction equations which results in corrections to C_L , C_D , C_m , and all other coefficients. This correction method does not account for movement of the model closer to the wall with increasing angle of attack during T478. Flow angularity is not known and has not been applied to any of the data.

III. Repeatability Analysis Results and Discussions

A. Repeatability Analysis Method

The repeatability analysis used in this paper is the method of regression statistical analysis described and used by Wahls, et al.¹⁴ This method uses a least squares polynomial curve fit based on all of the data points. The data were separated into different alpha ranges and various orders of polynomial curve fits were used. The basis for choosing the alpha range and the curve fit order was based on evaluating the residuals between each data point and the curve fit and minimizing the error over the alpha range.

The data scatter range was then assessed by calculating the scatter about this curve fit. This method uses the concept of prediction intervals to determine the bounds about the curve fit. These prediction intervals state that for a certain confidence level (95% for these analyses) any future data point will be within these bounds.

All data used for the repeatability analysis for config 1 were acquired at a Mach number of 0.20, Reynolds numbers of 4.1 to 4.6 million, and include only increasing angles of attack i.e., data where hysteresis was observed is not included in the repeatability analysis. Angle of attack, α , was selected as the independent variable for this analysis because the CFD cases for HiLiftPW-1 are defined at fixed angle of attack.

Also, for all data in this analysis the BLRS was used to reduce the size of the boundary layer on the tunnel floor and there is no artificial transition on the model. All data also include wall corrections to correct to "free-air". Some of the data acquisition during T506 and T513 involved staying on condition for a period of time while either hot film data or PIV data were acquired. Typically several force/moment data points were taken during this time and those back-to-back points were averaged together to make one point for this analysis.

It must be noted that there is evidence of bias in the data and this bias violates the statistical principle of randomness of the data. Nonetheless, the prediction intervals are believed to be useful for defining the scatter for this set of data.

B. Instrumentation

Forces and moments were measured with a strain gauge, 5-component semi-span balance installed under the floor in the 14x22. As mentioned previously, different balances were used for T478 and T506/T513. The MC-60 balance (6,000 pounds normal force capability) was used for T478, but some of the moments were overloaded during the test and this prevented taking the model to $C_{L,max}$ for several configurations. Some of the T478 data for config 1 were obtained through stall prior to the realization of the overloading issue. The data were examined post-test and it was determined that the overload data were still good and useful. Very little of the overload data were outside of the calibration range of the balance. Prior to T506, the MC-110 balance (11,000 pound normal force capability) was gauged and calibrated for use during both T506 and T513 so there would be no problem with taking the model to stall.

The model angle of attack was measured by an optical system. There were several infrared emitters potted into the surface of the nose and cameras in the ceiling sensed their locations and angle of attack was calculated from their positions.

The 14x22 tunnel conditions including the tunnel dynamic pressure were measured by the standard 14x22 tunnel instrumentation.

An uncertainty analysis was completed for these tests. The uncertainty analysis was based on the instrumentation uncertainties and used propagation of errors through the data reduction equations. Comparisons between the instrumentation uncertainty analysis and the repeatability analysis will be discussed in the force and moment repeatability sections.

C. Force and Moment Repeatability - Long Term (between tests)

This long-term repeatability analysis for config 1 in the 14x22 contains data from T478 in 1998, T506 in 2002, and T513 in 2003. The known differences between T478, T506, and T513 discussed in the experimental investigation descriptions above are summarized in Table 3.

Table 3. Differences between T478, T506, and T513 entries.

test	date	flap overlap	balance	tunnel position	BLRS surface	misc
478	Sept 1998	0.005	MC-60	balance center at tunnel station 15.56 feet	old grating	wall slots not sealed old fan drive
506	Aug 2002	0.0026	MC-110	balance center at tunnel station 17.75 feet	new grating	wall slots sealed new fan drive hot films on model
513	Mar 2003	0.0026	MC-110	balance center at tunnel station 17.75 feet	new grating	wall slots sealed new fan drive

Another difference between the tests that may affect repeatability is the tunnel temperature variation. The tunnel temperature is not controlled and the difference in ambient temperature at different times of the year results in a slight variation in Reynolds number. This small range of Reynolds number (4.1 million to 4.6 million) is included in this analysis.

One important factor to consider in the long-term repeatability analysis is changes to the rigging of the flap and the slat. During T478 there was a re-rigging to config 1 during the test for both the slat and the flap. Prior to T506 the slat and flap rigging were set and this rigging was not changed or moved until after T513. Just as a reminder, slat settings were all the same and the flap deflection and gap were the same, but there was a difference in flap overlap between T478 and T506/T513.

Figure 4 shows the long-term repeatability for Trap Wing config 1 in the 14x22 for C_L vs. α . This is separated into four alpha ranges for different curve fits. The prediction interval over the linear part of the C_L - α curve is ± 0.028 . For $\alpha < 1^\circ$ and α 's approaching stall and post-stall the prediction intervals increase and the data show more variation as expected for regions where separation is occurring on the model. Also, the different polars in Fig. 4 show a variation in the stall angle between $\alpha \sim 34.5^\circ$ and $\alpha \sim 36^\circ$. Figure 5 shows the residuals for C_L vs. α between the curve fit and each individual point. Looking at the residuals it is easier to see where the biases are between the different tunnel entries.

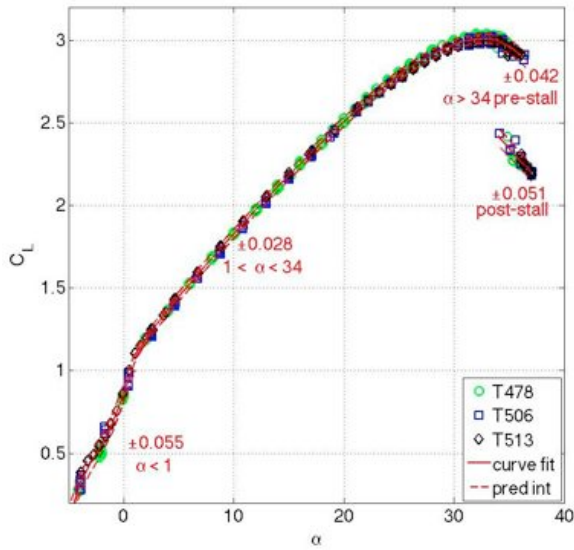


Figure 4. C_L vs. α long-term repeatability at $M = 0.20$.

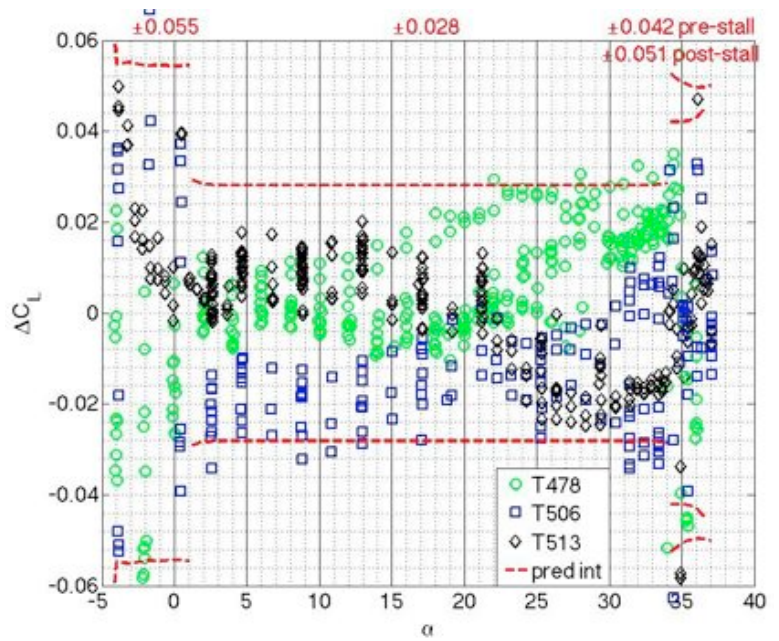


Figure 5. C_L vs. α residuals.

A plot of pitching moment vs. angle of attack is where the biases between the tests are most evident. Figure 6 shows the C_m variation with α and Fig. 7 shows the residuals between each point and the curve fit. The C_m curve fits were separated into three ranges: $\alpha < 1^\circ$, $\alpha > 1^\circ$ and pre-stall, and post-stall. Looking at Fig. 6 or Fig. 7, T506 is offset from T478 and T513 for $0^\circ < \alpha < 20^\circ$. But for $20^\circ < \alpha < 33^\circ$, T478 is offset from T506 and T513. These offsets may be due to the hot films on the model for T506 and/or the difference in flap overlap between T478 and T506/T513.

Figure 7 shows that C_m is fairly consistent within a given test. This same type of analysis with only T478 data shows the C_m prediction interval for $\alpha > 1^\circ$ to stall is ± 0.005 . This is one third of the interval for the combined tests.

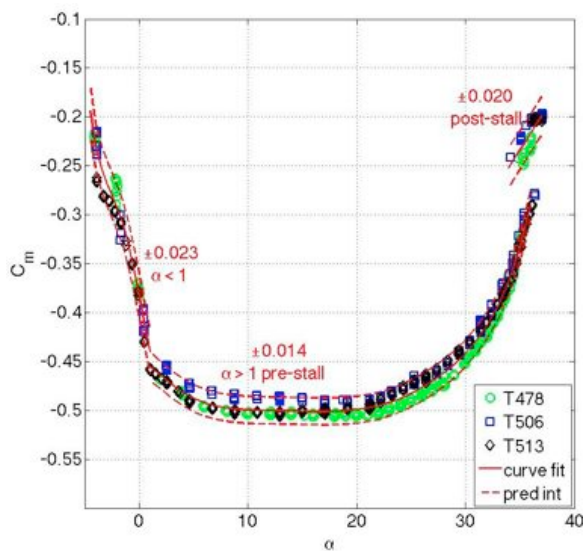


Figure 6. C_m vs. α long-term repeatability at $M = 0.20$.

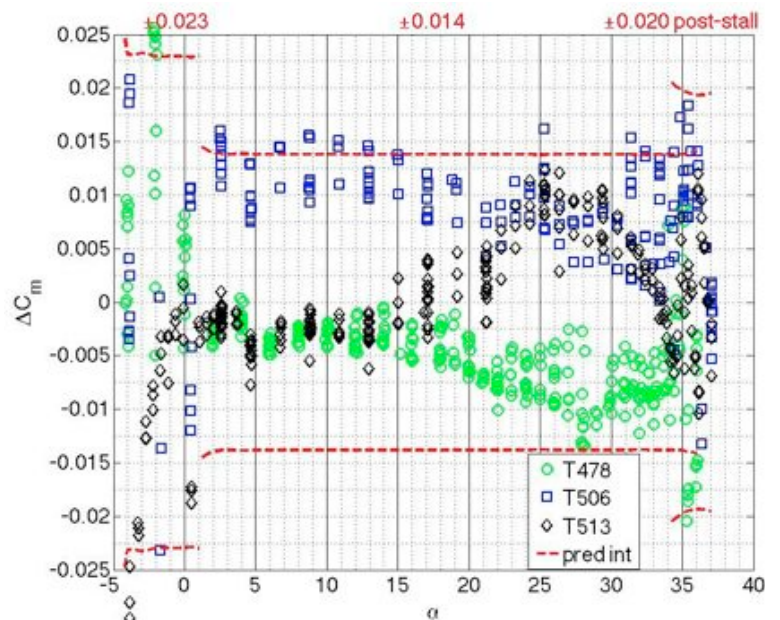


Figure 7. C_m vs. α residuals.

Figure 8 shows the C_D variation with α and Fig. 9 shows the residuals. The drag coefficient shows biases between the tests also. At the lower angles of attack the drag prediction interval is about 50 counts. T478 is consistently higher in C_D than T506 and T513 and the delta becomes larger with increasing α up to stall. Because of the larger spread in the data as angle of attack is increased, these curve fits are divided into six α ranges. The trend of the C_D data is different than seen in Fig. 7 for C_m . For C_D , T506/T513 are more consistent with each other over the α range. But for C_m , the trend for T506/T513 is dissimilar in the lower α range but similar in the higher α range (see Fig. 7). The reason for the different behaviors is not known.

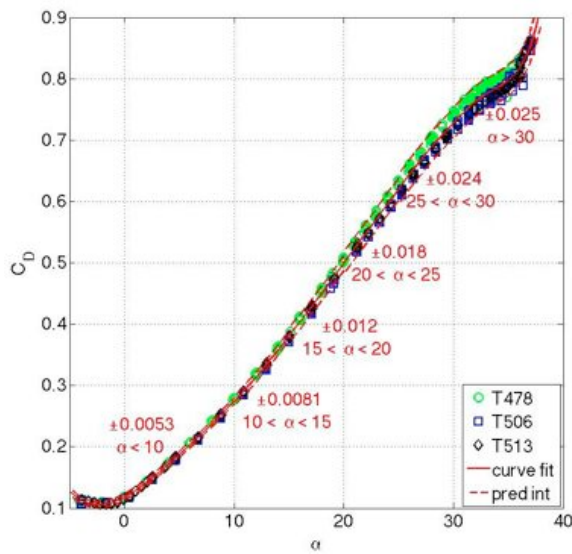


Figure 8. C_D vs. α long-term repeatability at $M = 0.20$.

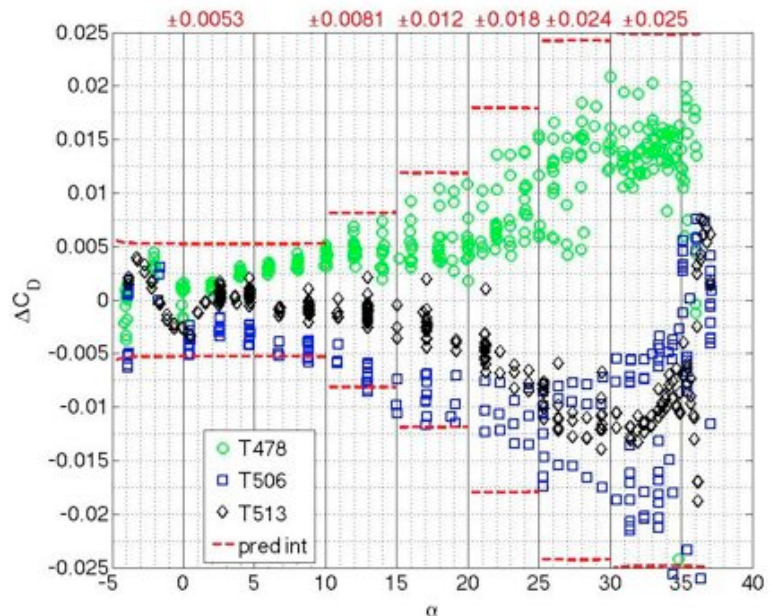


Figure 9. C_D vs. α residuals.

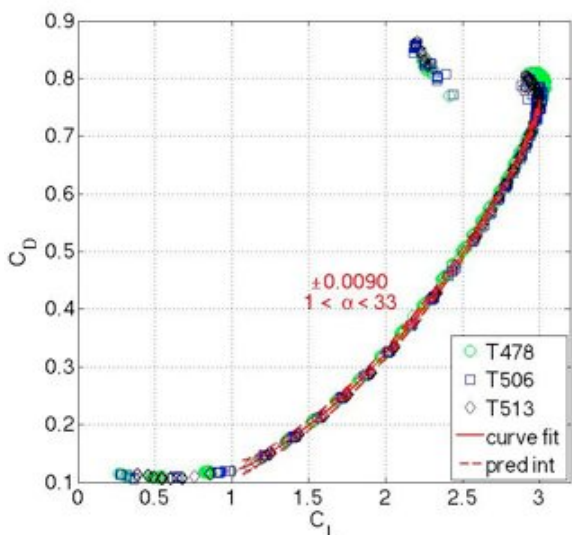


Figure 10. C_D vs. C_L long-term repeatability at $M = 0.20$.

Figure 10 shows the C_D prediction intervals if C_L is the independent variable instead of α . This curve fit was done over the range of $1^\circ < \alpha < 33^\circ$. This shows a smaller prediction interval than when using α as the independent variable. The C_D prediction interval using C_L is ± 0.0090 , whereas the interval with α varies from ± 0.0053 to ± 0.0240 over a similar range of data points. Using C_L as the independent variable leads to a much smaller C_D interval.

This smaller prediction interval leads to the conclusion that the measurements themselves are better than the analysis using α seems to indicate. That is, the differences between the data from the three tests at a given α are due to more than just measurement uncertainties.

C_m was also evaluated with C_L as the independent variable. That evaluation shows the prediction intervals on the same order as the prediction intervals with α as the independent variable.

The overall variations in this long-term analysis are about 2-3 times larger than the expected instrumentation uncertainty levels. The repeatability analysis for a single

test indicates the variation is much closer to the expected instrumentation uncertainty. This indicates that there are more factors contributing to the variation between all the tests than just the instrumentation. While it is fairly straight forward to calculate expected instrumentation uncertainty for a given test by using propagation of errors through the data reduction equations for C_L , C_D , and C_m , it is much more difficult to identify and quantify factors that contribute to overall uncertainty or to long-term variation without performing multiple tests.

If the goal of the second experimental investigation was just to see how well the force and moment data could repeat on this model, several of the modified items would not have been changed. But the goal was not to repeat data, it was to collect more flow physics data and to improve the testing techniques used for testing this model. In other words, lessons learned from the 1998 test and improvements made to the facility were used to improve the testing techniques in subsequent tests.

D. Force and Moment Repeatability - Short-Term (within a test)

Figures 4 through 9 clearly show that each individual test has a smaller band of scatter than the band of scatter for all three tests together. To illustrate short-term variability, Fig. 11 shows C_L vs. α for Test 478 only and Fig. 12 shows the residuals from the curve fit to each point. Over the linear region of the curve, the prediction interval is ± 0.018 compared to the ± 0.028 for the combined tests (Fig. 4). The T478 data consist of four sets of polars taken using config 1 over a time frame of two weeks. Each set includes two to four back-to-back polars. T478 started with config 1 and during the test there was one change to the flap rigging and one change to the slat rigging and then the model was returned to config 1. Despite these model changes, the within-test prediction intervals for C_L are on the same order as that expected due to instrumentation uncertainty. This level of within-test variability is the same for C_D and C_m , which are not shown, and less than the long-term analysis, which was 2-3 times larger than the instrumentation uncertainty.

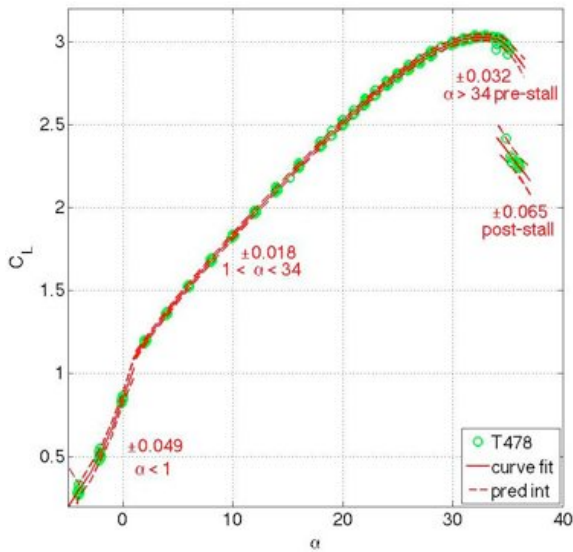


Figure 11. C_L vs. α short-term repeatability at $M = 0.20$.

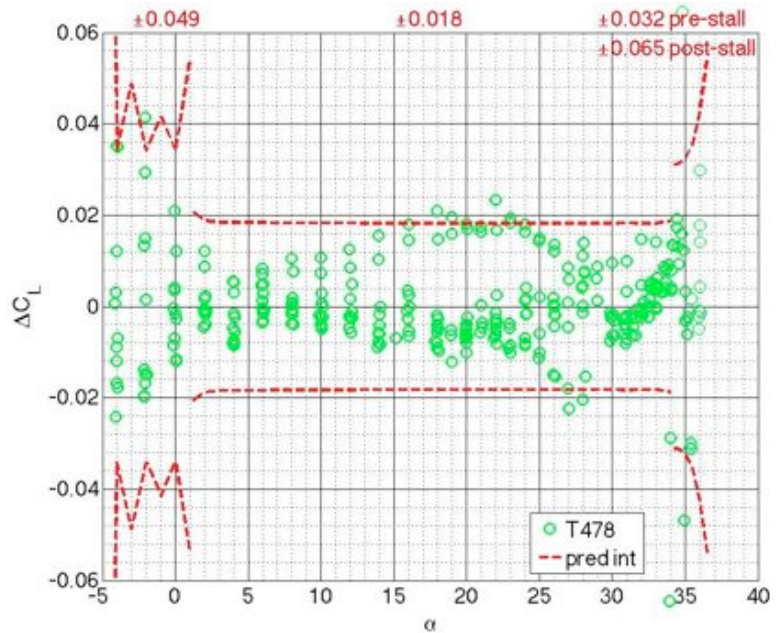


Figure 12. C_L vs. α short-term residuals.

IV. Velocity Profiles Results and Discussion

A. Probe and Traversing Hardware

A significant part of the 1998/1999 experimental investigation was the measurement of velocity profiles using 7-hole probes to examine the mean, off-body flow field. The probe measurements made during the 14x22 entry were used primarily for risk reduction and to downselect configurations prior to testing in the 12 Foot tunnel. The number of useful profiles obtained is limited due to problems with the traversing system that included the instrumentation system and wiring and installation of the traverser onto the Trap Wing model. After the 14x22 entry, an extensive effort was undertaken to address these issues prior to the 12 Foot entry. This work also included photogrammetric measurements of the flap and main element with the probe installed and at various positions of probe travel. This work was required to define where the probe tip was relative to the flap or main element and the orientation of the probe to properly transform the velocity components.



Figure 13. Forward probe at $\eta = 15\%$ as mounted in the 14x22.

The velocity profiles were acquired using two traversing mechanisms: one for the leading edge of the main element (forward traverser) and one for the aft end of the main element and flap positions (aft traverser). The forward traverser was contained in the main element except for a small portion of the traversing stem extending slightly below the lower surface. Figure 13 shows the probe and probe stem of the forward probe.

The aft traverser was more intrusive due to the thinness of the aft side of the main element and the flap. Figure 14 shows the lower surface side of the model in the 14x22 with the traversing system installed on the main element at $\eta = 83\%$. Figure 15 shows the 7-hole probe on the upper surface of the main element at $\eta = 83\%$. The following is a description of the aft traversing system from Ref. 3:

A major challenge in the design of a traverser for a complex, three-dimensional flow field is to minimize aerodynamic intrusiveness and relative motion between the probe tip and model. Four legs attached a teardrop-shaped motor fairing to the model lower surface. The probe stem protruded through the model, and the probe surveyed the model upper surface at discrete spanwise and streamwise locations. Two fairings shrouded the probe stem on the model lower surface, and were individually yawed to minimize loading on the fairing. The local orientation of the motor fairing (sideslip angle) varied with spanwise location, and was chosen to minimize intrusiveness based on three-dimensional panel code solutions.

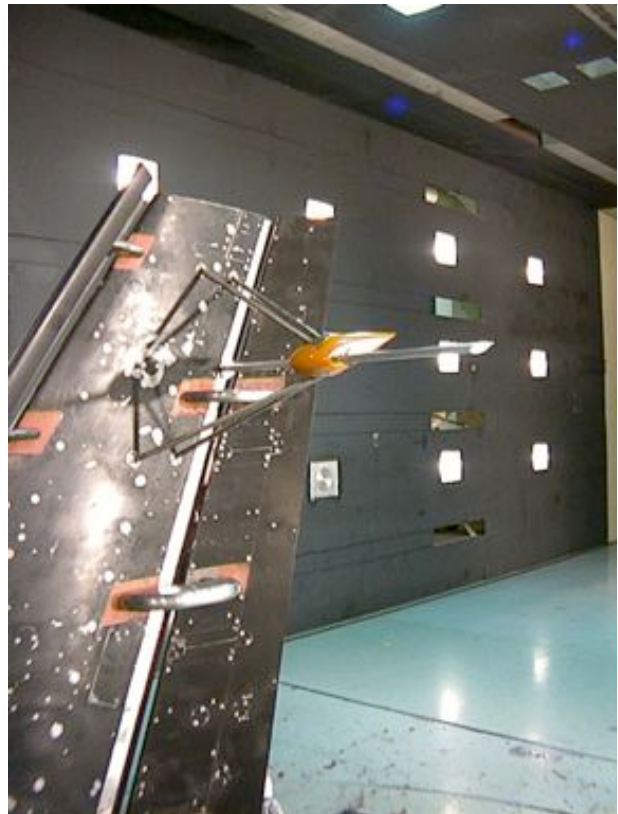


Figure 14. Aft traverser installed on main element at $\eta = 83\%$.

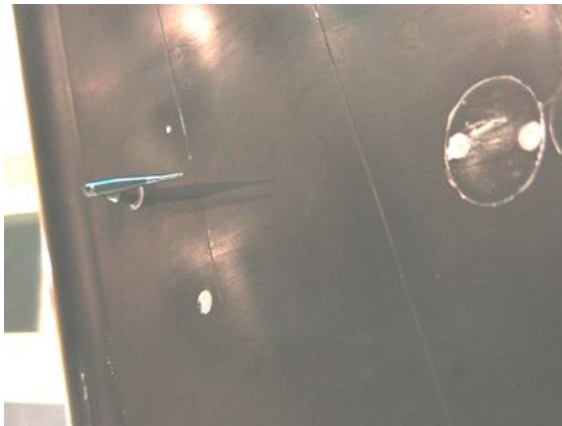


Figure 15. 7-hole probe on main element at $\eta = 83\%$.

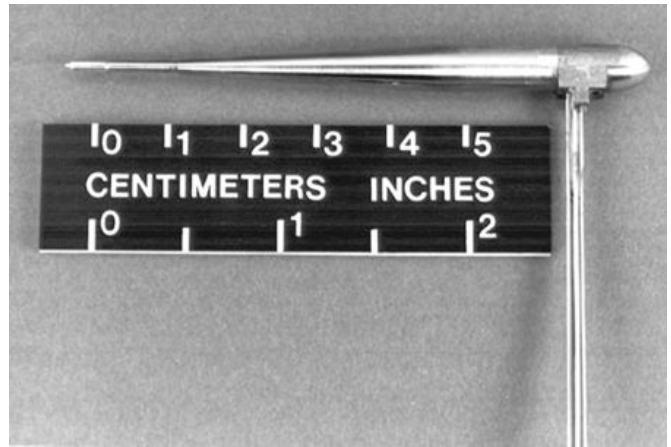


Figure 16. 7-hole probe.

Probe details and calibration information are also taken from Ref. 3:

Seven-hole probes were purchased from Texas A & M University and calibrated in the Probe Calibration Tunnel of the Flow Physics and Control Branch at NASA-Langley. At the tip, the probes were 0.065 inch in diameter (see Figure 16).

The probes were calibrated at three total pressure ($P_t=17, 32, 60$ psia), from Mach 0.10 to 0.80 in increments of 0.10. The angular range of calibrations extended from -20 to $+20$ degrees in 2 degree increments (in both α and β), and from -20 to -56 degrees and $+20$ to $+56$ degrees in 4 degree increments. Approximately 24 test conditions/probe, and 1431 data points/test condition were acquired.

The data reduction procedure divided the probe face into 7 sectors, and data was reduced using recent least-squares¹⁵ and neural-net methods.¹⁶

The profiles presented here were reduced with the least-squares method. This method was chosen because it was more efficient and there is little difference between the two methods.

The probe pressures were measured with electronic pressure scanners. The forward probe used a scanner with a range of ± 10 psi and the aft probe used a scanner with a range of ± 5 psi. The accuracy of the scanners is $\pm 0.10\%$ of full scale.

Table 4. Velocity profile locations at 14x22.

	η	location	traverser	α	probe heights, h_{probe} (inches)
A	15%	main element	forward	28	0.98 - 2.23
B	83%	main element	aft	28	0.68 - 8.68
C	83%	flap - front	aft	10, 28	0.08 - 8.03
D	83%	flap - aft	aft	10, 20, 28	0.08 - 4.03

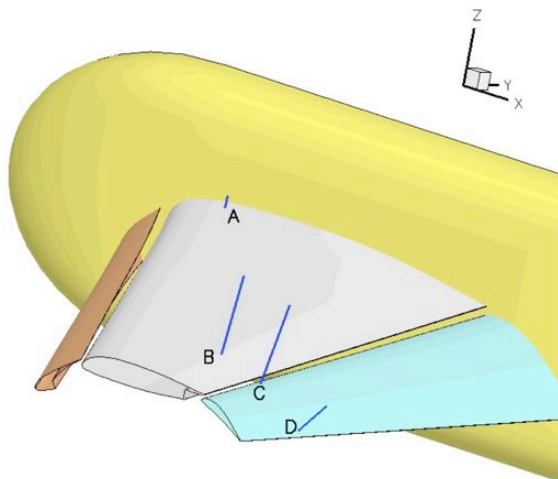


Figure 17. Velocity profile locations. Note that the support brackets are not shown in this figure.

The locations of the seven profiles measured on config 1 during T478 are identified in Fig. 17. Table 4 provides specific details regarding the probe location along with the angle of attack and range of probe heights above the surface where data were taken. The measured probe heights are normal to the local surface.

All of the mean velocity profile data are available on the HiLiftPW website. With one exception the data include individual velocity components and measurement locations in model coordinates. At $\eta = 15\%$ ("A" in Fig. 17) only the velocity magnitudes are provided. The probe mounting hardware for this location was modified between the 14x22 and 12 Foot entries to get closer to the surface. Also, the photogrammetry data used to determine probe position and orientation were only taken of the modified mount. Therefore, because the orientation of the probe is not

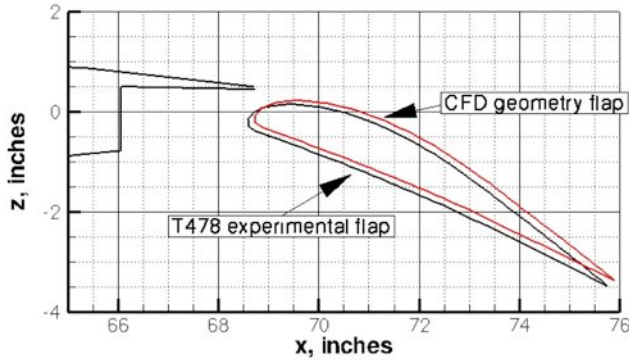


Figure 18. Differences at $\eta = 83\%$ in flap overlap between experiment setup and HiLiftPW-1 CFD geometry.

accurately known, the velocity components could not be calculated.

There is one note of caution with respect to the velocity profiles. There are differences in the flap overlap settings between the T478 experiment and the CFD geometry used for the HiLiftPW-1. The experimental overlap (o/c) is 0.005 (Test 478) along the span and the CFD geometry varies from $o/c = 0.0046$ at $\eta = 13\%$ to $o/c = 0.0001$ at $\eta = 80\%$. Figure 18 shows the difference in overlap at $\eta = 83\%$. The experimental overlap is 0.005 (Test 478) and at this η , the CFD overlap is approximately 0. It is unknown what this difference in overlap has on the viscous phenomena of the flow field.

B. Mean Velocity Data

Because of the three-dimensionality of this flow field and the limited number of velocity profiles, it is difficult to explain some of the features seen in the velocity profiles. At $\eta = 83\%$ the tip vortex is having a greater influence on the local flow field, especially as angle of attack is increased. There is also some evidence that the outboard slat bracket wake may have an effect on the profiles at $\eta = 83\%$. From surface flow visualization pictures (not shown) on the main element, we determined that the outboard slat bracket (located at $\eta = 94\%$) wake travels inboard. It was difficult to follow the exact trajectory, but it did pass close to the $\eta = 85\%$ pressure row on the aft portion of the main element. There are no pictures of the surface flow on the flap to indicate how this bracket wake interacts with the flap. Results from the HiLiftPW showed the effect of including the brackets was significant on the flap surface pressures.²

The profiles shown in Figs. 19-22 have been non-dimensionalized by the free-stream velocity, V_∞ . These profiles were acquired at a Mach number of 0.20, Reynolds number of approximately 4.2×10^6 , and the 14x22 BLRS was used to reduce the size of the floor boundary layer.

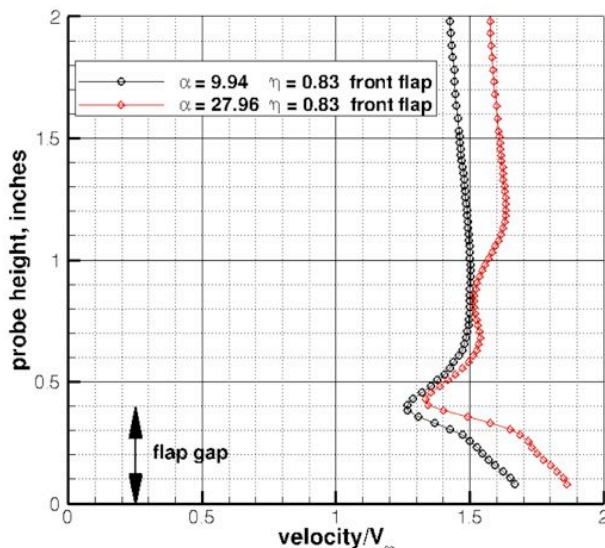


Figure 19. Velocity profiles at $\eta = 83\%$, forward on flap, for $\alpha = 10^\circ$ and 28° . $M = 0.20$, $Re_c = 4.2 \times 10^6$.

Figure 19 shows profiles of velocity magnitude at $\eta = 83\%$ at the front of the flap for $\alpha = 10^\circ$ and 28° (this is "C" in Fig. 17). Velocity profiles are measured normal to the surface and the first point is less than one inch behind the leading edge of the flap. Note that this location is on the forward part of the flap and the gap is approximately 0.4 inches at this location. The profiles here are shown from 0.08 to 2 inches above the surface; there are no significant structures seen in these profiles above 2 inches. In these profiles the slot flow is seen in the higher velocities between the surface and 0.4 inches. For $\alpha = 10^\circ$ and $\alpha = 28^\circ$ the main element wake can be seen around $h_{probe} = 0.4$ inches. There is no evidence of the slat wake in the mean flow in the $\alpha = 10^\circ$ data. An additional wake, probably from the slat, can be seen in the $\alpha = 28^\circ$ data around $h_{probe} = 0.8$ inches.

Figure 20 shows profiles of velocity magnitude at $\eta = 83\%$ at the rear of the flap for $\alpha = 10^\circ$, 20° , and 28° (this is "D" in Fig. 17). The first point of the profile is approximately 7 inches behind the leading edge of the flap. The probe heights for this position are between 0.08 inches and 4 inches. The $\alpha = 10^\circ$ profile includes some of the flap boundary layer to approximately $h_{probe} = 0.6$ inches, then what appears to be the main element wake with a minimum at approximately

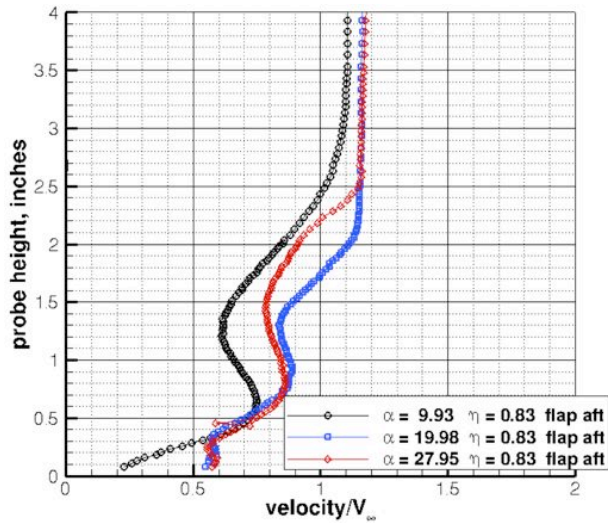


Figure 20. Velocity profiles at $\eta = 83\%$, aft on flap, for $\alpha = 10^\circ, 20^\circ,$ and 28° . $M = 0.20, Re_c = 4.2 \times 10^6$.

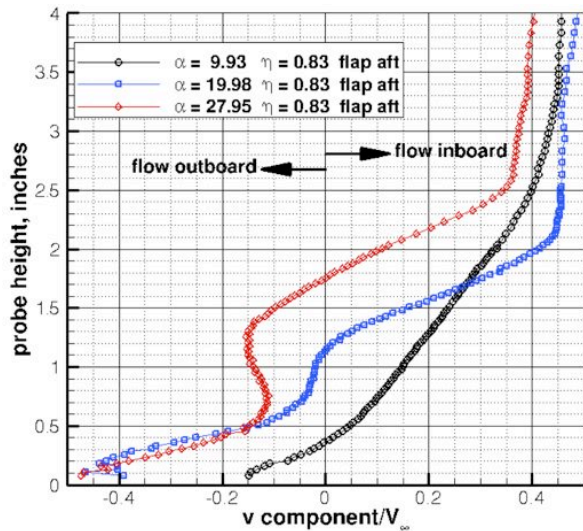


Figure 21. Spanwise velocity component profiles at $\eta = 83\%$, aft on flap, for $\alpha = 10^\circ, 20^\circ,$ and 28° . $M = 0.20, Re_c = 4.2 \times 10^6$.

$h_{probe} = 1.3$ inches. Both the $\alpha = 20^\circ$ and 28° profiles show the velocity magnitude to be relatively constant from $h_{probe} = 0.08$ inches to about 0.3 inches. Above $h_{probe} = 0.3$ inches the profiles for $\alpha = 20^\circ$ and 28° capture some of the flap boundary layer. The $\alpha = 20^\circ$ profile shows a wake with a minimum about $h_{probe} = 1.3$ inches, whereas the $\alpha = 28^\circ$ profile shows a wake that is spreading or perhaps merging. Another feature worth noting is the significant decrease in velocity between the aft flap profiles and the forward flap profiles.

Figure 21 shows the spanwise component, v , of the profiles shown in Fig 20. There is a strong spanwise flow near the surface towards the wing tip for the aft flap position. Negative v is flow outboard towards the tip and positive v is flow inboard. This outboard spanwise flow gets stronger and extends more into the flow field with increasing angle of attack. For $\alpha = 10^\circ$ the outboard flow extends to $h_{probe} = 0.35$ inches. For $\alpha = 20^\circ$ this outboard flow extends to $h_{probe} = 1.1$ inches and for $\alpha = 28^\circ$ to 1.7 inches. Close to the surface the outboard spanwise flow has increased to almost half the free-stream velocity. The flow angles here are near the limits of the calibrated range of the probe.

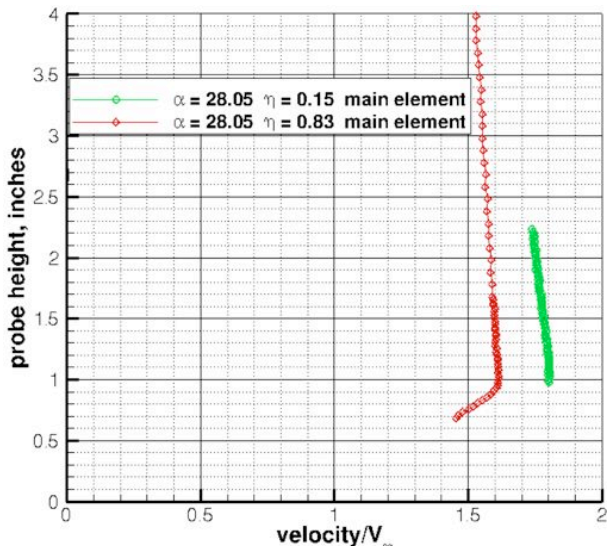


Figure 22. Velocity profiles on the main element at $\eta = 15\%$ and $\eta = 83\%$. $M = 0.20, Re_c = 4.2 \times 10^6$.

Figure 22 shows the two main element profiles acquired at $\alpha = 28^\circ$. These are the only profiles available that are away from the flap overlap issue discussed previously between the experiment and the HiLiftPW-1 CFD geometry. The first profile is inboard at $\eta = 15\%$ and the first point is approximately 6 inches behind the leading edge of the main element (this is "A" on Fig. 17). Note that this profile starts about one inch above the surface. It appears to have missed the slat wake, but it can still be useful for future CFD comparisons. As mentioned previously, during the 14x22 entry the probe at this position was unable to get close to the surface. This deficiency was corrected prior to the 12 Foot entry. The second profile in Fig. 22 is at $\eta = 83\%$ and the first point is approximately 15 inches behind the leading edge of the main element (this is "B" in Fig. 17). The lower part of this profile, $h_{probe} < 1.0$ inches, has captured the upper portion of what is most likely the slat wake.

As noted in Ref. 3, there are localized effects of the aft traverser on the surface pressures. For the $\eta = 83\%$ positions these effects extend out to the tip. The effect of the traversing systems on the integrated forces was also

evaluated. With the exception of C_D at $\alpha = 10^\circ$, the C_L , C_m , and C_D with the aft traverser on are within the prediction intervals given in Fig. 5, 7, and 9. At $\alpha = 10^\circ$, the C_D is higher than the prediction interval by approximately 30 drag counts.

V. Conclusion

Renewed interest in the Trap Wing database for the first High-Lift Prediction Workshop provided an opportunity to continue examining the experimental data acquired during a series of tests conducted in 1998 and 2002-2003. Part of this examination included a long-term repeatability analysis of the aerodynamic forces acquired in the 14x22. This analysis was included in the first High-Lift Prediction Workshop for use by the CFD community. This analysis has shown that performing an uncertainty analysis on the instrumentation alone may be suitable for determining “short-term” or within test variability but this approach can significantly underestimate “long-term” variability. In this case, the “long-term” variability, for a given angle of attack, was found to be 2-3 times greater than the measurement uncertainty based solely on instrumentation. There are known changes during the testing that contributed to the “long-term” variability.

Another part of the data examination was the completion of the velocity profile reduction. Velocity profile data for the 14x22 entry are now available to the research community on the HiLiftPW website. There are two special sessions planned for the 30th AIAA Applied Aerodynamics Conference in June 2012 that will include CFD comparisons to this newly available data. In the future, this work will be extended to make the more extensive set of velocity profiles acquired over a range of Reynolds numbers from the 12 Foot entry available to the CFD community.

References

- ¹Slotnick, J. P., Hannon, J. A., and Chaffin, M., "Overview of the First AIAA CFD High Lift Prediction Workshop (Invited)," AIAA-2011-862, *49th AIAA Aerospace Sciences Meeting*, Orlando, FL, Jan. 4-7, 2011.
- ²Rumsey, C. L., Long, M., Stuever, R. A., and Wayman, T. R., "Summary of the First AIAA CFD High Lift Prediction Workshop (Invited)," AIAA-2011-939, *49th AIAA Aerospace Sciences Meeting*, Orlando, FL, Jan. 4-7, 2011.
- ³Johnson, P. L., Jones, K. M., and Madson, M. D., "Experimental Investigation of a Simplified 3D High Lift Configuration in Support of CFD Validation," AIAA-2000-4217, *18th AIAA Applied Aerodynamics Conference and Exhibit*, Denver, CO, Aug. 14-17, 2000.
- ⁴Khorrami, M. R., Berkman, M. E., Li, F., and Singer, B. A., "Computational Simulations of a Three-Dimensional High-Lift Wing," AIAA-2002-2804, *20th AIAA Applied Aerodynamics Conference*, St. Louis, MO, June 24-26, 2002.
- ⁵Streett, C. L., Casper, J. H., Lockard, D. P., Khorrami, M. R., Stoker, R. W., Elkoby, R., Wenneman, W. F., and Underbrink, J. R., "Aerodynamic Noise Reduction for High-Lift Devices on a Swept Wing Model," AIAA-2006-212, *44th AIAA Aerospace Sciences Meeting*, Reno, NV, Jan. 9-12, 2006.
- ⁶Gentry, G. L., Quinto, P. F., Gatlin, G. G., and Applin, Z. T., "The Langley 14- by 22-Foot Subsonic Tunnel: Description, Flow Characteristics, and Guide for Users," NASA TP-3008, 1990.
- ⁷Rogers, S. E., Roth, K., and Nash, S. M., "Validation of Computed High-Lift Flows with Significant Wind-Tunnel Effects," *AIAA Journal*, Vol. 39, No. 10, Oct. 2001, pp. 1884-1892.
- ⁸Neuhart, D. H., and McGinley, C. B., "Free-Stream Turbulence Intensity in the Langley 14- by 22-Foot Subsonic Tunnel," NASA TP-2004-213247, 2004.
- ⁹McGinley, C. B., Jenkins, L. N., Watson, R. D., and Bertelrud, A., "3-D High-Lift Flow-Physics Experiment - Transition Measurements," AIAA-2005-5148, *AIAA Fluid Dynamics Conference and Exhibit*, Toronto, Ontario, June 6-9, 2005.
- ¹⁰Watson, R. D., Jenkins, L. N., Yao, C., McGinley, C. B., Paschal, K. B., and Neuhart, D. H., "PIV Measurements in the 14x22 Low Speed Tunnel: Recommendations for Future Testing," NASA TM-2003-212434, 2003.
- ¹¹Iyer, V., Kuhl, D. D., and Walker, E. L., "Improvements to Wall Corrections at the NASA Langley 14X22-Ft Subsonic Tunnel," AIAA-2003-3950, *21st AIAA Applied Aerodynamics Conference*, Orlando, FL, June 23-26, 2003.
- ¹²Herriot, J. G., "Blockage Corrections For Three-Dimensional-Flow Closed-Throat Wind Tunnels, With Consideration of the Effect of Compressibility," NACA Report 995, 1950.
- ¹³Rae, W. H., Jr., and Pope, A., *Low-Speed Wind Tunnel Testing*, 2nd ed., John Wiley & Sons, New York, 1984, Chaps. 6.
- ¹⁴Wahls, R. A., Adcock, J. B., Witkowski, D. P., and Wright, F. L., "A Longitudinal Aerodynamic Data Repeatability Study for a Commercial Transport Model Test in the National Transonic Facility," NASA TP 3522, 1995.
- ¹⁵Rediniotis, O. K. and Kinser, R. E., "Development of a Nearly Omnidirectional Velocity Measurement Pressure Probe," *AIAA Journal*, Vol. 36, No. 10, Oct. 1998, pp. 1854-1860.
- ¹⁶Rediniotis, O. K. and Vijayagopal, R., "Miniature Multihole Pressure Probes and Their Neural-Network-Based Calibration," *AIAA Journal*, Vol. 37, No. 6, June 1999, pp. 666-674.